J|A|C|S
ARTICLES
Published on Web 07/13/2006

Exploration of Ground and Excited Electronic States of Aromatic and Quinoid *S,S*-Dioxide Terthiophenes. Complementary Systems for Enhanced Electronic Organic Materials

Juan Casado,[†,#] Marek Z. Zgierski,[†] Paul C. Ewbank,[‡] Michael W. Burand,[‡] Daron E. Janzen,[‡] Kent R. Mann,[‡] Ted M. Pappenfus,[§] Anna Berlin,[||] Ezequiel Pérez-Inestrosa,[⊥] Rocío Ponce Ortiz,[○] and Juan T. López Navarrete*,[○]

Contribution from the Steacie Institute for Molecular Sciences, National Research Council of Canada, K1A 0R6, Ottawa, Canada, Department of Chemistry, University of Minnesota, Minneapolis, Minnesota 55455, Division of Science and Mathematics, University of Minnesota, Morris, Minnesota 56267, Istituto CNR di Scienze e Tecnologie Molecolari, via C. Golgi 19, 20133 Milano, Italy, Department of Organic Chemistry, University of Málaga, Campus de Teatinos s/n, Málaga 29071, Spain, and Department of Physical Chemistry, University of Málaga, Campus de Teatinos s/n, Málaga 29071, Spain

Received February 27, 2006; E-mail: teodomiro@uma.es

Abstract: We analyze the electronic and molecular structures for the ground and excited electronic states of aromatic terthiophene (**3T**), the quinodimethane 3′,4′-dibutyl-5,5′′-bis(dicyanomethylene)-5,5′′-dihydro-2,2′:5′,2′′-terthiophene (**3Q**), and isologues with the middle ring S-oxidized (**3TO2**, **3QO2**). These represent extremes of electron rich and deficient ground states, often exhibiting complementary properties. Oxidizing the central sulfur atom affects the molecular structure, electron affinity, and photophysical properties of both π systems. The consequences for **3T** include de-aromatization of the central thiophene, red-shifting of the electronic absorption spectrum, and lowering of the reduction potential. The electron deficient quinoid **3QO2** shows an enhancement of electron affinity from reducing the electron-donor ability of sulfur, and a blue-shifting of its electronic absorption spectrum was seen. Fluorescence emission is quenched in the sulfonated terthiophene, and the contrary effect again would be expected upon sulfonation of a quinoid emitter. Raman vibrational spectroscopy, electrochemistry, and UV−vis and fluorescence spectroscopies are analyzed in conjunction with theoretical calculations.

I. Introduction

The demand for new organic molecular materials with improved electrical and optical properties necessitates extensive experimental and theoretical investigations of underlying structure−property relationships. Electroluminescent devices, for instance, require materials (small molecules or polymers) that are not only fluorescent but also electroactive with high electron affinities.[1] Among organic conjugated materials, oligothiophenes are advantageous due to their great chemical stability and their ease and variety of functionalization.[2] Conventional unsubstituted or alkyl substituted α,α′-connected thiophene oligomers, 2−7 rings long, display good photoluminescence efficiencies in solution but are quenched in the solid state.[3−5] These photophysical features have been further improved by substitution with fluorescence enhancing groups such as phenyl,[6] biphenyl,[7] fluorene,[8] bis(methylphenyl)aminophenyl,[9] bis(9,9-dimethylfluorenyl)aminophenyl,[10] etc. Bearing in mind the focus of electroluminescent properties, they are poor electron conductors lacking low energy electrochemical reductions.

A promising concept of inserting thienyl *S,S*-dioxides in oligothiophenes to afford solid state luminescence efficiency

† National Research Council of Canada.
‡ University of Minnesota, Minneapolis.
§ University of Minnesota, Morris.
|| Istituto CNR di Scienze e Tecnologie Molecolari.
⊥ Department of Organic Chemistry, University of Málaga.
○ Department of Physical Chemistry, University of Málaga.
Permanent address: Department of Physical Chemistry, University of Málaga.

(1) For example, see: (a) Kraft, A.; Grimsdale, A. C.; Holmes, A. B. *Angew. Chem., Int. Ed.* **1998**, *37*, 42. (b) Mitschke, U.; Bauerle, P. *J. Mater. Chem.* **2000**, *10*, 1471. (c) Heeger, A. J. *Solid State Commun.* **1998**, *107*, 673. (d) Kulkarmi, A. P.; Tonzola, C. J.; Babel, A.; Jenekhe, S. A. *Chem. Mater.* **2004**, *16*, 4556. (e) Richter, M. M. *Chem. Rev.* **2004**, *104*, 3003. (f) Armstrong, N. R.; Wightman, R. M.; Gross, E. M. *Annu. Rev. Phys. Chem.* **2001**, *52*, 391. (g) Fungo, F.; Wong, K.-T.; Ku, S.-Y.; Hung, Y.-Y.; Bard, A. J. *J. Phys. Chem. B* **2005**, *109*, 3984. (h) Yan, H.; Lee, P.; Armstrong, N. R.; Graham, A.; Evmenenko, G. A.; Dutta, P.; Marks, T. J. *J. Am. Chem. Soc.* **2005**, *127*, 3172. (i) Perepichka, I. F.; Perepichka, D. F.; Meng, H.; Wudl, F. *Adv. Mater.* **2005**, *17*, 1.
(2) *Handbook of Oligo- and Polythiophenes*; Fichou, D., Ed.; Wiley-VCH: Weinheim, 1998. *Handbook of conductive polymers*; Skotheim, T. A.; Elsenbaumer, R. L.; Reynolds, J. R. Eds.; Marcel Dekker: New York, 1998. *Electronic Materials: The Oligomeric Approach*; Müllen, K.; Wegner, G., Eds.; Wiley-VCH: Weinheim, 1998. Barbarella, G.; Sotgiu, G. *Adv. Mater.* **2005**, *17*, 1581.
(3) (a) Becker, R. S.; Seixas de Melo, J.; Macanita, A. L.; Elisei, F. *Pure Appl. Chem.* **1995**, *67*, 9. (b) Grebner, D.; Helbig, H.; Rentsch, S. *J. Phys. Chem.* **1995**, *99*, 16998. (c) Becker, R. S.; Seixas de Melo, J.; Macanita, A. L.; Elisei, F. *J. Phys. Chem.* **1996**, *100*, 18683. (d) Janssen, A. J.; Smilowitz, L.; Sariciftci, S. N.; Moses, D. *J. Chem. Phys.* **1994**, *101*, 1787. (e) Hotta, S.; Waragai, K. *J. Phys. Chem.* **1993**, *97*, 7427. (e) Rubio, M.; Merchán, M.; Ortí, E. *ChemPhysChem* **2005**, *6*, 1357.

10.1021/ja061372w CCC: $33.50

and increased electron affinity has been studied extensively by G. Barbarella et al.[11] This strategy has allowed the fabrication of highly efficient electroluminescent diodes based on polyalkylated quinquethiophene *S*,*S*-dioxides.[12] Furthermore, the optimal balance in the optical and electrical properties by inclusion of *S*,*S*-dioxides in oligothiophenes is found for alternating oxidized/nonoxidized units in the chain, and this will be part of our approach in this work.[11]

Recently, quinoidal oligothiophenes were reported with exceptionally high electron affinities (i.e., net two-electron reductions close-to-zero vs the Ag/AgCl reference electrode).[13] This feature underlies their extremely efficient actuation as n-channel semiconductors in FET devices.[14] Some examples

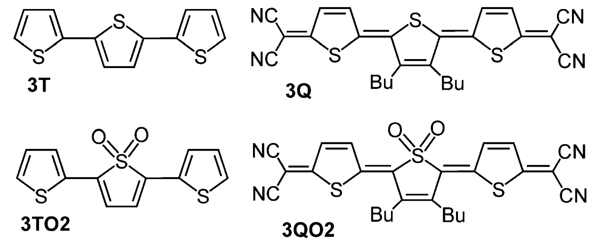

Figure 1. Chemical structures and nomenclature of the studied compounds.

were also ambipolar hole and electron transporters, operating at both a positive and negative bias.[14] Dicyanomethylene end-capping of the oligothiophene core is an efficient way to stabilize electron deficient quinoidal forms by intramolecular charge transfer.[15]

With respect to their photophysical properties, quinoidal oligothiophenes have been studied little so far. To the best of our knowledge only one sulfonated quinoid analogue, derived from dithieno[3,2-*b*:2′,3′-*d*]thiophene, has been reported and electrochemically characterized.[16] The present study offers thorough physical characterization and theoretical analysis of a family of oligothiophenes, allowing assessment of *S*-oxidation on both aromatic and quinoid forms. In the field of organic electroluminescent and lighting materials, a key objective is ambipolar electroluminescent compounds able to conduct electron and hole charge defects simultaneously. In this regard, quinoidal systems are bipolar materials themselves, and the achievement of even a low emission regime would be quite significant (i.e., actual amorphous oligothiophenes are poor bipolar conductors but efficient emitters). Assuming that *S*,*S*-dioxides may improve fluorescence emission, it is meritorious to shed light about the molecular foundation of the redox and luminescent properties in aromatic and quinoidal sulfonated oligothiophenes. This study constitutes a distinct perspective for the development of new organic electroluminescent materials and presents a guide for their engineering.

To this end, we will analyze four conjugated terthiophenes (Figure 1). The pair of terthiophene **3T** and its *S*,*S*-dioxide derivative **3TO2** will be used to address the effect on aromatic systems. The second pair, the quinoidal terthiophene **3Q** and its corresponding *S*,*S*-dioxide **3QO2**, examines the effect in quinoidal systems. The study is divided into two main parts. The first analyzes the electronic consequences of sulfur oxidation in both aromatic and quinoidal forms. The main tool for probing ground electronic state features will be Raman spectroscopy, while electrochemistry allows us to study the modulation of electron affinity. The second part of the paper studies excited states by UV−vis electron absorption and emission spec-

(4) (a) Garnier, F. *Acc. Chem. Res.* **1999**, *32*, 209. (b) Horowitz, G.; Delannoy, P.; Bouchriha, H.; Deloffre, F.; Fave, J. L.; Garnier, F.; Hajlaoui, R.; Heyman, M.; Kouki, F.; Valet, P.; Wintgens, V.; Yassar, A. *Adv. Mater.* **1994**, *6*, 752. (c) Marks, R. N.; Muccini, M.; Lunedi, E.; Michel, R. H.; Murgia, M.; Zamboni, R.; Taliani, C.; Horowitz, G.; Garnier, F.; Hopmeier, M.; Oestreich, M.; Mahrt, R. F. *Chem. Phys.* **1998**, *227*, 49. (d) Dippel, O.; Brandtl, V.; Bassler, H.; Danieli, R.; Zamboni, R.; Taliani, C. *Chem. Phys. Lett.* **1993**, *216*, 418. (e) Bongiovanni, G.; Botta, C.; Brédas, J. L.; Cornil, J.; Ferro, D. R.; Mura, A.; Piaggi, A.; Tubito, R. *Chem. Phys. Lett.* **1997**, *278*, 146. (f) Beljonne, D.; Cornil, J.; Brédas, J. L.; Friend, R. H. *Synth. Met.* **1996**, *76*, 61. (g) Garnier, F.; Horowitz, G.; Valat, P.; Kouki, F.; Wintgens, V. *Appl. Phys. Lett.* **1998**, *72*, 2087. (h) Birnbaum, D.; Fichou, D.; Kohler, B. *J. Chem. Phys.* **1992**, *96*, 165. (i) Hapiot, P.; Demanze, F.; Yassar, A.; Garnier, F. *J. Phys. Chem.* **1996**, *100*, 8397. (j) Garcia, P.; Pernaut, J. M.; Happiot, P.; Wintgens, V.; Valat, P.; Garnier, F.; Delabouglise, D. *J. Phys. Chem.* **1993**, *97*, 513. (k) Barbarella, G.; Zanelli, L.; Gigli, A.; Mazzeo, M.; Anni, M.; Bongini, A. *Adv. Funct. Mater.* **2005**, *15*, 664.

(5) (a) Cornil, J.; dos Santos, D. A.; Beljonne, D.; Brédas, J. L. *J. Phys. Chem.* **1995**, *99*, 5604. (b) Demanze, F.; Cornil, J.; Garnier, F.; Horowitz, G.; Valat, P.; Yassar, A.; Lazzaroni, R.; Brédas, J. L. *J. Phys. Chem. B* **1997**, *101*, 4553. (c) Kohler, A.; Beljonne, D. *Adv. Funct. Mater.* **2004**, *14*, 11. (d) Cornil, J.; dos Santos, D. A.; Crispin, X.; Silbey, R.; Brédas, J. L. *J. Am. Chem. Soc.* **1998**, *120*, 1289. (e) Beljonne, D.; Shuai, Z.; Pourtois, G.; Brédas, J. L. *J. Phys. Chem. A* **2001**, *105*, 3899. (f) Wasserberg, D.; Marsat, P.; Meskers, S. C. J.; Janssen, R. A. J.; Beljonne, D. *J. Phys. Chem. B* **2005**, *109*, 4410.

(6) Ichikawa, M.; Hibino, R.; Inoue, M.; Haritani, T.; Hotta, S.; Araki, K.-I.; Koyama, T.; Taniguchi, Y. *Adv. Mater.* **2005**, *17*, 2073.

(7) Ichikawa, M.; Hibino, R.; Inoue, M.; Haritani, T.; Hotta, S.; Koyama, T.; Taniguchi, Y. *Adv. Mater.* **2003**, *15*, 213. Nagawa, M.; Hibino, R.; Hotta, S.; Yanagi, H.; Ichikawa, M.; Koyama, T.; Taniguchi, Y. *App. Phys. Lett.* **2002**, *80*, 544.

(8) Meng, H.; Zheng, J.; Lovinger, A. J.; Wang, B.-C.; Van Patten, G. P.; Bao, Z. *Chem. Mater.* **2003**, *15*, 1778. Wong, K.-T.; Wang, C.-F.; Chou, C. H.; Su, Y. O.; Lee, G.-H.; Peng, S. M. *Org. Lett.* **2002**, *4*, 4429.

(9) Noda, T.; Imae; I.; Noma, N.; Shirota, Y. *Adv. Mater.* **1997**, *9*, 239. Noda, T.; Ogawa, H.; Noma, N.; Shirota, Y. *Adv. Mater.* **1997**, *9*, 720. Noda, T.; Ogawa, H.; Noma, N.; Shirota, Y. *Appl. Phys. Lett.* **1997**, *70*, 699. Noda, T.; Ogawa, H.; Noma, N.; Shirota, Y. *J. Mater. Chem.* **1999**, *9*, 2177.

(10) Shirota, Y.; Kinoshita, M.; Noda, T.; Okumoto, K.; Takahiro, O. *J. Am. Chem. Soc.* **2000**, *122*, 11021. Doi, H.; Kinoshita, M.; Kumoto, K.; Shirota, Y. *Chem. Mater.* **2003**, *15*, 1080.

(11) For example, see: (a) Barbarella, G.; Favaretto, L.; Zambianchi, M.; Pudova, O.; Arbizanni, C.; Bongini, A.; Mastragostino, M. *Adv. Mater.* **1998**, *10*, 551. Barbarella, G.; Favaretto, L.; Sotgiu, G.; Zambianchi, M.; Antolini, L.; Pudova, O.; Bongini, A. *J. Org. Chem*. **1998**, *63*, 5497. (b) Barbarella, G.; Zambianchi, M.; Antolini, L.; Ostoja, P.; Maccagnani, P.; Bongini, A.; Marseglia, E. A.; Tedesco, E.; Gigli, G.; Cingolani, R. *J. Am. Chem. Soc.* **1999**, *121*, 8920. (c) Barbarella, G.; Favaretto, L.; Sotgiu, G.; Zambianchi, M.; Fattori, V.; Cocchi, M.; Cacialli, F.; Gigli, G.; Cingolani, R. *Adv. Mater.* **1999**, *11*, 1375. (d) Antolini, L.; Tedesco, E.; Barbarella, G.; Favaretto, L.; Sotgiu, G.; Zambianchi, M.; Casarini, D.; Gigli, G.; Cingolani, R. *J. Am. Chem. Soc.* **2000**, *122*, 9006. (e) Arbizzani, C.; Barbarella, G.; Bongini, A.; Favaretto, L.; Mastragostino, M.; Ostoja, P.; Pudova, O.; Zambianchi, M. *Opt. Mater.* **1998**, *9*, 43. (f) Barbarella, G.; Pudova, O.; Arbizzani, C.; Mastragostino, M.; Bongini, A. *J. Org. Chem.* **1998**, *63*, 1742. (g) Barbarella, G.; Favaretto, L.; Sotgiu, G.; Antolini, L.; Gigli, G.; Cingolani, R.; Bongini, A. *Chem. Mater.* **2001**, *13*, 4112. (h) Tedesco, E.; Della Sala, F.; Favaretto, L.; Barbarella, G.; Albesa-Jové, D.; Pisignano, D.; Gigli, G.; Cingolani, R.; Harris, K. D. M. *J. Am. Chem. Soc.* **2003**, *125*, 12277. (j) Camaioni, N.; Ridolfi, G.; Fattori, V.; Favaretto, L.; Barbarella, G. *Appl. Phys. Lett.* **2004**, *84*, 1901. (k) Mazzeo, M.; Vitale, V.; Della Santa, F.; Anni, M.; Barbarella, G.; Favaretto, L.; Sotgiu, G.; Cingolani, R.; Gigli, G. *Adv. Mater.* **2005**, *17*, 34.

(12) For example, see: (a) Gigli, G.; Barbarella, G.; Favaretto, L.; Cacialli, F.; Cingolani, R. *App. Phys. Lett.* **1999**, *75*, 439. (b) Gigli, G.; Inganas, O.; Anni, M.; De Vittorio, M.; Cingolani, R.; Barbarella, G.; Favaretto, L. *Appl. Phys. Lett.* **2001**, *78*, 1493. (c) Zavelanni-Rossi, M.; Lanzani, G.; De Silvestri, S.; Anni, M.; Gigli, G.; Cingolani, R.; Barbarella, G.; Favaretto, L. *Appl. Phys. Lett.* **2001**, *79*, 4082. (d) Pisignano, D.; Anni, M.; Gigli, G.; Cingolani, R.; Zavelanni-Rossi, M.; Lanzani, G.; Barbarella, G.; Favaretto, L. *Appl. Phys. Lett.* **2002**, *81*, 3534.

(13) (a) Casado, J.; Miller, L. L.; Mann, K. R.; Pappenfus, T. M.; Higuchi, H.; Ortí, E.; Milián, B.; Pou-Amérigo, R.; Hernández, V.; López Navarrete, J. T. *J. Am. Chem. Soc.* **2002**, *124*, 12380. (b) Pappenfus, T. M.; Raff, J. D.; Hukkanen, E. J.; Burney, J. R.; Casado, J.; Drew, S. M.; Miller, L. L. *J. Org. Chem.* **2002**, *67*, 6015. (c) Janzen, D. E.; Burand, M. W.; Ewbank, P. C.; Pappenfus, T. M.; Higuchi, H.; da Silva Filho D. A.; Young, V. G.; Brédas, J. L.; Mann, K. R. *J. Am. Chem. Soc.* **2004**, *126*, 15295.

(14) Pappenfus, T. M.; Chesterfield, R. J.; Frisbie, C. D.; Mann, K. R.; Casado, J.; Raff, J. D.; Miller, L. L. *J. Am. Chem. Soc.* **2002**, *124*, 4184. Chesterfield, R. J.; Newman, C. R.; Pappenfus, T. M.; Ewbank, P. C.; Haukaas, M. H.; Mann, K. R.; Miller, L. L.; Frisbie, C. D. *Adv. Mater.* **2003**, *15*, 1278.

(15) Casado, J.; Pappenfus, T. M.; Mann, K. R.; Ortí, E.; Viruela, P. M.; Milián, B.; Hernández, V.; López Navarrete, J. T. *ChemPhysChem* **2004**, *5*, 529. Hernández, V.; Hotta, S.; López Navarrete, J. T. *J. Chem. Phys.* **1998**, *109*, 2543. Hernández, V.; Calvo Losada, S.; Higuchi, H.; López Navarrete, J. T. *J. Phys. Chem. A* **2000**, *104*, 661.

(16) Yui, K.; Ishida, H.; Aso, Y.; Otsubo, T.; Ogura, F.; Kawamoto, A.; Tanaka, J. *Bull. Chem. Soc. Jpn.* **1989**, *62*, 1547.

Scheme 1. Synthesis of **3QO2**

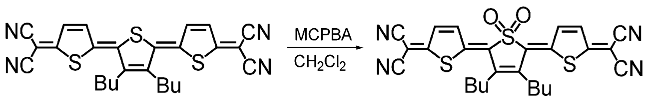

troscopies. This delineates the photophysical properties, allowing predictions of molecules that efficiently combine electron affinity with fluorescence response. All the experimental data in this paper are supported by theoretical calculations in the framework of the Density Functional Theory for ground-state properties and Time-Dependent Density Functional Theory for excited states.

II. Experimental Section

A. General Synthetic Considerations. 3-Chloroperoxybenzoic acid (MCPBA) was purchased from Aldrich and used as received. ^{1}H NMR spectra were recorded on a Varian Unity (300 MHz) spectrometer and were referenced to the residual chloroform peak (7.27 ppm). Mass spectra were obtained on a Finnigan MAT95 spectrometer. The remaining oligomers were synthesized according to literature methods: **3T**;[17] **3TO2**;[17] **3Q**.[13b]

B. Synthesis of 2,2′-[(3,4-Dibutyl-1,1-dioxo-2,5-thiophenediylidene)-bis-5,2-thiophenediylidene]bis-propanedinitrile (3QO2, Scheme 1). The synthesis is similar to one employed by Yui et al. in the oxidation of a quinoid dithienothiophene.[16] Selectivity for the center ring is the reverse of that observed in aromatic systems.[11f] In our experience, yields > 50% could be achieved in a few hours. In an open Erlenmeyer flask containing **3Q** (137 mg, 0.28 mmol) in dichloromethane (30 mL) was added MCPBA (0.325 g, 77% max, 1.45 mmol). The resulting mixture was stirred for 4 days and then partitioned between CH_2Cl_2 and saturated aqueous sodium bicarbonate. The organic layer was separated, dried with $MgSO_4$, filtered, and concentrated to afford a crude solid. This was purified by column chromatography (silica gel) using CH_2Cl_2 as the eluent. The product was recovered as a violet band to afford 121 mg (83%) of **3QO2** as a violet solid. ^{1}H NMR (CD_2Cl_2): δ 8.11 (d, 2H, $J = 6.0$ Hz), 7.48 (d, 2H, $J = 6.0$ Hz), 2.74 (t, 4H), 1.58 (m, 8H), 1.05 (t, 6H). HRCIMS $C_{26}H_{22}N_4O_2S_3$ calcd, 518.0905; found, 518.0897.

C. Experimental Details. NMR data were collected on a Varian 300 MHz instrument. The chemical shifts are reported in ppm, and the coupling constants (J) are reported in Hz. CD_2Cl_2 is referenced to the residual proton peak (5.32 ppm). Cyclic voltammetry data were collected on a BAS 100B electrochemical analyzer. Potentials are reported vs aqueous Ag/AgCl and are not corrected for the junction potential. FT-Raman spectra were measured using an FT-Raman accessory kit (FRA/106-S) of a Bruker Equinox 55 FT-IR interferometer. A continuous-wave Nd:YAG laser working at 1064 nm was employed for excitation. A germanium detector operating at liquid nitrogen temperature was used. Raman scattering radiation was collected in a backscattering configuration with a standard spectral resolution of 4 cm^{-1}. To avoid possible damage to samples upon laser radiation, its power was kept at a level lower than 100 mW and 1000−3000 scans were averaged for each spectrum. Absorption and emission spectra were obtained in CH_2Cl_2 or THF. UV−vis−NIR absorption spectra were recorded on either a Lambda 19 Perkin-Elmer dispersive spectrophotometer or an Agilent 8453 instrument equipped with a diode array detection system. Emission spectra were measured using a JASCO FP-750 spectrofluorometer. No fluorescent contaminants were detected upon excitation in the wavelength region of experimental interest. Solutions were prepared with an absorbance between 0.1 and 0.2 at the wavelength region of experimental interest.

D. X-ray Structure Determination. Crystals of **3QO2**/CH_2Cl_2 solvate were obtained by slow evaporation of CH_2Cl_2 solution. Data were collected at the X-ray Crystallographic Laboratory, Department of Chemistry, University of Minnesota. A crystal (approximate dimensions $0.5 \times 0.15 \times 0.05$ mm^3) was placed onto a glass fiber and mounted on a Siemens SMART Platform for data collection at 173(2) K using graphite monochromated Mo Kα radiation ($\lambda = 0.710\,73$ Å). A randomly oriented region of reciprocal space was surveyed to the extent of 1.5 hemispheres and to a resolution of 0.84 Å. Three major sections of frames were collected with 0.30° steps in ω at 3 different ϕ settings. The intensity data were corrected for absorption and decay (SADABS).[18a] Space groups were determined on the basis of systematic absences and intensity statistics. Direct-methods solutions provided the positions of most non-hydrogen atoms. Several full-matrix least-squares/difference Fourier cycles were performed to locate the remaining non-hydrogen atoms. All calculations were performed using SHELXTL.[18b] The final full matrix least squares refinement converged to $R1 = 0.0375$ and $wR2 = 0.0800$ (F^2, all data).

E. Theoretical Details. In recent years, density functional theory methods have become very popular. It is clear that DFT methods have many advantages; for example, they scale well with system size and implicitly include electron correlation effects, and the accuracy of DFT methods is comparable to that of correlated ab initio procedures, such as MP2, which do not scale as well.[19] In general these methods are ideal low-cost computational procedures to analyze conjugated molecules in which the electron correlation effect becomes an important task. Regarding their ab initio counterparts, DFT methods are also advantageous and successful in describing vibrational properties in large molecules.[20] Hence, in this work the ground-state total energies, equilibrium geometries, eigenfrequencies, and normal coordinates were calculated within the framework of density functional theory by means of the Gaussian 03 package of programs.[21] Calculations were performed using Becke's hybrid three-parameter exchange functional (B3) combined with the nonlocal correlation functional of Lee, Yang, and Parr (LYP).[22] The Gaussian atomic basis sets cc−pVDZ (correlation-consistent polarized valence double-ζ) were used.[23] Molecular orbital contours were plotted using Molekel 4.3.[24] The following constraints were assumed for the model: (i) Optimal geometries were determined on isolated entities in a vacuum. (ii) To reduce the computational problem ethyl groups instead of butyl groups were considered, with the assumption that omitted distal atoms insignificantly influence the electron distribution in the π-system. (iii) No conformational restrictions were imposed, and inter-ring dihedral angles were freely rotatable. (iv) For the resulting ground-state optimized geometries, harmonic vibrational frequencies and Raman intensities were calculated numerically. (v) DFT calculations yield vibrational frequencies with an accuracy of about 10% compared to the respective experimental values. Calculated harmonic vibrational frequencies are uniformly scaled by a single scaling factor (0.96) to improve the numerical comparison.[25] All quoted theoretical vibrational frequencies reported are thus scaled values.

The time-dependent DFT (TD-DFT) approach is widely applied to describe electron excitations.[26] Though not as accurate for excitations

(17) Berlin, A.; Zotti, G.; Zecchin, S.; Schiavon, G.; Cocchi, M.; Virgili, D.; Sabatini, C. *J. Mater. Chem.* **2003**, *13*, 27.
(18) (a) An empirical correction for absorption anisotropy: Blessing, R. *Acta Crystallogr.* **1995**, *A51*, 33. (b) *SHELXL*, V.6.1; Bruker AXS: Madison, WI, 2001.
(19) Stephens, P. J.; Devlin, F. J.; Chabalowski, F. C. F.; Frisch, M. J. *J. Phys. Chem.* **1994**, *98*, 11623. Novoa, J. J.; Sosa, C. *J. Phys. Chem.* **1995**, *99*, 15837. Casida, E.; Jamorski, C.; Casida, K. C.; Salahub, D. R. *J. Chem. Phys.* **1998**, *108*, 4439. Stratman, R. E.; Scuseria, G. E.; Frisch, M. J. *J. Chem. Phys.* **1998**, *109*, 8218.
(20) Bertsch, G. F.; Smith, A.; Yabana, K. *Phys. Rev. B* **1995**, *52*, 7876. Francl, M. M.; Pietro, W. J.; Hehre, W. J.; Binkley, J. S.; Gordon, M. S.; Defrees, D. J.; Pople, J. A. *J. Chem. Phys.* **1982**, *77*, 3654.
(21) Frisch, M. J. et al. *Gaussian 03*, revision B.05; Gaussian, Inc.: Pittsburgh, PA, 2003.
(22) Becke, A. D. *J. Chem. Phys.* **1993**, *98*, 1372.
(23) Woon, D. E.; Dunning, T. H., Jr. *J. Chem. Phys.* **1993**, *98*, 1358. Kendall, R. A.; Dunning, T. H., Jr.; Harrison, R. J. *J. Chem. Phys.* **1992**, *96*, 6796.
(24) Portmann, S.; Lüthi, H. P. *Chimia* **2000**, *54*, 766.
(25) Scott, A. P.; Radom, L. *J. Phys. Chem.* **1996**, *100*, 16502.
(26) Runge, E.; Gross, E. K. U. *Phys. Rev. Lett.* **1984**, *52*, 997. Gross, E. K. U.; Kohn, W. *Adv. Quantum Chem.* **1990**, *21*, 255. Heinze, H.; Goerling, A.; Roesch, N. *J. Chem. Phys.* **2000**, *113*, 2088.

as the ordinary DFT is for ground properties, the theory has considerable predictive power and is computationally quite tractable. This allows calculations for large molecules. Vertical electronic excitation energies and oscillator strengths were computed by using the TD-DFT approach. At least the 30 lowest-energy electronic excited states were computed for all the molecules. TD-DFT calculations were carried out using the same functional and basis set as those in the previously optimized molecular geometries.

III. X-ray Structure, Raman Spectra, and Ground-Electronic State Properties

A. Thiophene Aromaticity and π-Electron Conjugation. It is instructive to clarify a principal concept used in succeeding sections regarding the structure of oligothiophene derivatives in their ground electronic states. Thiophene is a five-membered aromatic ring. Although *aromaticity* is not an observable property several criteria have been invoked to account numerically for it.[27] We are mainly concerned with the structural criterion reflecting the averaging of bond lengths, essentially the averaged difference between the successive long and short carbon−carbon bonds in a conjugated path (Bond Length Alternation; BLA) with benzene as the prototypical case where the BLA is zero. In thiophene, one of the two lone electron pairs of the sulfur atom participates in ring aromatization. With this assumption, any polarization of the electron density out of the five-member ring disrupts its aromaticity. This occurs to some extent when thiophenes are connected through the α, ω positions to yield linear oligothiophenes in which aromatic character competes with linear oligoene-*like* inter-ring C═C/C−C conjugation. Taking these arguments in mind, the ring BLA values in a given oligothiophene, evaluated with respect to that of isolated thiophene (i.e., 0.063 Å by DFT//B3LYP/cc-pVDZ calculations), contain information about the electronic structure of the thiophene ring, and thus the aromatic/quinoidal character and electronic substituents interactions may be evaluated. In this context, this work will deal with BLA data to evaluate the aromaticity/quinoidal distribution, while Raman spectroscopy will provide experimental proof of this electronic structure.

B. Solid-State Structure of 3QO2. The structure consists of a quinoidal dicyanomethylene-capped terthiophene with two oxygen atoms double-bonded to the middle thiophene sulfur atom and two *n*-butyl groups appended to the center thiophene ring (Figure 2 and Table 1). The structure also contains one molecule of methylene chloride as a solvate.

The π-system of **3QO2** is quite flat with a mean deviation from planarity of 0.180 Å, as calculated from a least-squares plane. Each molecule packs with one butyl group oriented above and one below the thiophene plane, stacked with parallel molecular orientation into monotonic, weakly associated (3.920 Å) slipped π-stacks. This contrasts with the structure of **3Q** where each molecule orients both butyl groups on the same face of the thiophene plane and forms strongly associated antiparallel dimers that further stack with slight alternation in distance between adjacent molecules (3.466 Å vs 3.559 Å).[13] Notably, the steric shielding of the central ring of **3QO2** precludes overlap at this point, necessitating a slip of about one-half the length of the molecule within the stack. Layers in the structure exist with all butyl groups pointing at each other (lipophilic) or only SO_2 units pointing toward each other (polar). This structure lacks the extended interactions between the π-conjugated systems that facilitate electron/hole conduction.[13] This could benefit light emission in the solid state as already shown for the class of *S,S*-dioxide oligothiophenes.[11]

(27) For example, see: Kertesz, M.; Choi, C. H.; Yang, S. *Chem. Rev.* **2005**, *105*, 3448. De Proft, F.; Geerlings, P. *Chem. Rev.* **2001**, *101*, 1451.

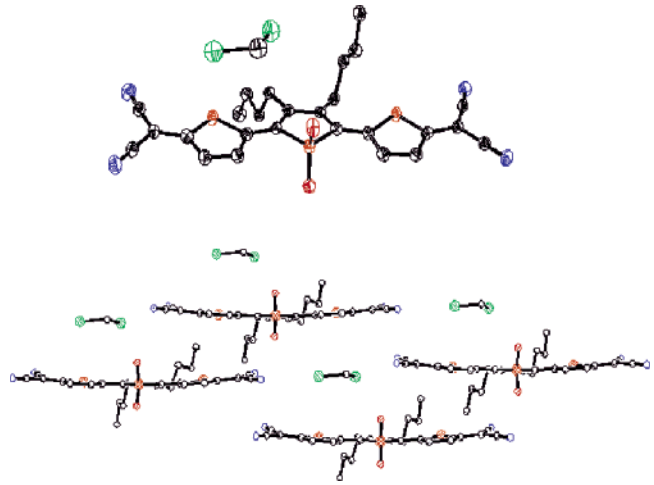

Figure 2. ORTEP and stacking diagram of the **3QO2** CH_2Cl_2 solvate. H atoms are omitted for clarity.

Table 1. X-ray Data Collection and Refinement

formula	$C_{26}H_{22}N_4O_2S_3{\cdot}CH_2Cl_2$
habit	plate
color	purple
lattice type	triclinic
space group	$P\bar{1}$
a (Å)	9.8167(7)
b (Å)	10.4061(7)
c (Å)	14.8780(10)
α (deg)	104.9590(10)
β (deg)	91.7280(10)
γ (deg)	105.9620(10)
V (Å^3)	1403.33(17)
Z	2
fw (g/mol)	603.58
D_c (g/cm^3)	1.428
T (K)	173(2)
μ (mm^{-1})	0.488
F(000)	624
θ range (deg)	1.43−25.02
index ranges	$-11 \le h \le 11$, $-12 \le k \le 12$, $-16 \le l \le 17$
reflections collected	10 540
unique reflections	4933 [R(int) = 0.0257]
weighting factors[a] (a,b)	0.0311, 0.6545
transmission (max, min)	1.0000, 0.90689
data/restraints/parameters	4933/0/343
R_1, wR_2 ($I > 2\sigma(I)$)	0.0375, 0.0754
R_1, wR_2 (all data)	0.0525, 0.0800
GOF	1.038

[a] $w = [\sigma^2(F_o^2) + (aP)^2 + bP]^{-1}$, where $P = (F_o^2 + 2F_c^2)/3$.

C. Calculated Molecular Geometries and Raman Line Wavenumbers. Figure 3 displays the DFT//B3LYP/cc-pVDZ theoretical Raman and the experimental FT-Raman spectra of all investigated oligomers.

The comparison of calculated and experimental quantities is quite satisfactory both in wavenumber and in intensity, confirming the optimized geometries (Figure 3) and the vibrational eigenvectors as reliable predictions of solid-state structures and of the molecular dynamic. We concentrate on the vibrational assignments of the main 1700−1300 cm^{-1} Raman bands and

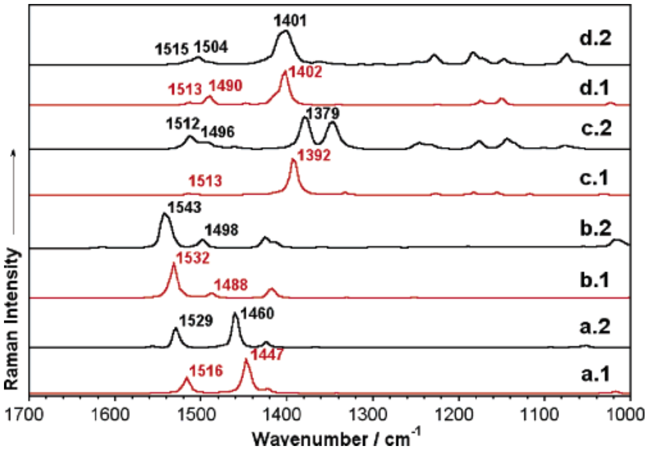

Figure 3. Theoretical (red, ".1") and FT-Raman spectra (black, ".2") of (a) **3T**, (b) **3TO2**, (c) **3Q**, and (d) **3QO2**. Ethyl groups instead of butyls are considered for the quinoid molecules.

how these change upon sulfonation based on theoretical geometries. The experimental Raman spectrum of **3T** is dominated by two lines at 1529 and 1460 cm^{-1}. The former band is due to an antisymmetric C═C ring stretching mode [ν_a(C═C), predicted at 1516 cm^{-1}] where the greatest vibrational amplitudes correspond to the terminal rings, whereas the latter, and strongest Raman scattering, arises from a symmetric C═C ring stretching mode [ν_s(C═C), predicted at 1447 cm^{-1}] of the central ring.[28] The ν_a(C═C) line in **3TO2** at 1543 cm^{-1} (predicted at 1532 cm^{-1}) is upshifted by 14 cm^{-1} with respect to **3T** becoming the most intense band of the spectrum. Changes are more dramatic for ν_s(C═C) which appears as a weak line at 1498 cm^{-1} in **3TO2** considerably upshifted by 38 cm^{-1} relative to **3T**. Therefore, selective oxidation of the central sulfur atom of **3T** gives rise to an inversion of the intensity pattern of the two most significant ν(C═C) lines followed by a sizable upshifting of their wavenumbers. Sulfonation is expected to extensively affect the features of the oxidized thiophene, but this also induces changes of the electronic structure of the conjoined rings. This has qualitatively been observed as the preferential ability to oxidize inner thiophene rings in large oligothiophenes.[11]

The spectroscopic data are clarified by examining the underlying structure. Experimental intramolecular bond lengths are not available for all four compounds, so a detailed comparison of their molecular structures is only possible accounting for theoretical optimized geometries. For **3TO2**, an averaged deviation of 0.007 Å (maximum of 0.016 and minimum of 0.002 Å) for the conjugated thienyl path is found between experimental and theoretical bond lengths, indicating good correlation between the gas-phase calculations and condensed phase structure.

Figure 4 displays the ground-state optimized B3LYP/cc-pVDZ bond distances and the BLA values for each ring of the four compounds under analysis. Based on these geometries, there exist two thiophene ring types in **3T** (i.e., a BLA of 0.048 Å

(28) Hernández, V.; Casado, J.; Ramírez, F. J.; Zotti, G.; Hotta, S.; López Navarrete, J. T. *J. Chem. Phys.* **1996**, *104*, 9271. Moreno Castro, C.; Ruiz Delgado, M. C.; Hernández, V.; Hotta, S.; Casado, J.; López Navarrete, J. T. *J. Chem. Phys.* **2002**, *116*, 10419. Casado, J.; Katz, H. E.; Hernández, V.; López Navarrete, J. T. *J. Phys. Chem. B* **2002**, *106*, 2488. Casado, J.; Miller, L. L.; Mann, K. R.; Pappenfus, T. M.; Hernández, V.; López Navarrete, J. T. *J. Phys. Chem. B* **2002**, *106*, 3597.

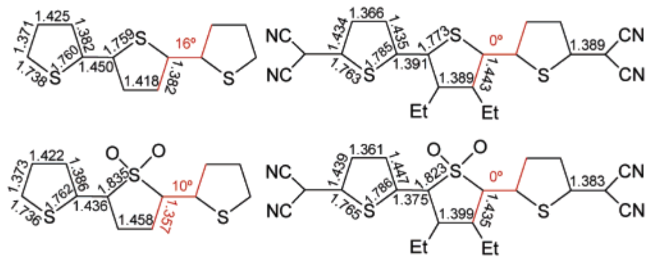

Figure 4. Ground electronic state B3LYP/cc-pVDZ optimized geometries. In red, dihedral angles.

for the two outermost rings and of 0.036 Å for the central one). Both are less aromatic than isolated thiophene (BLA = 0.063 Å), owing to the increase of inter-ring C═C/C─C conjugation which is most pronounced for the central ring (i.e., lowest BLA). Along with reduced aromaticity for the thienyl rings of **3T** there is elongation of the C─S bond distances. Once the ring character of the ν(C═C) vibrations has been recognized, the difference in the BLA values of each ring might correlate with their wavenumber peak position, namely, 0.048 Å/1529 cm^{-1} and 0.036 Å/1460 cm^{-1}.

Oxidation of the central sulfur removes the lone electrons from participation in ring aromaticity, as indicated by the lengthening of the C─S bonds of the sulfonated moiety (1.835/1.759 Å in **3TO2**/**3T**) and by the shortening/lengthening of the C═C/C─C in **3TO2** vs **3T**. This indicates increasing di-*ene* character of this central moiety at the expense of the aromatic thienyl feature. The strengthening of the double bonds on the central ring from 1.382 Å to 1.357 Å (**3T** vs **3TO2**) might explain the large displacement at higher energies of its ν_s(C═C) Raman band.

On the other hand, the slight BLA reduction from 0.048 Å to 0.042 Å for the terminal rings of **3TO2** vs **3T** anticipates a more moderate shifting of the ν_a(C═C) Raman scattering observed as a +14 cm^{-1}. Upon sulfonation two more structural events occur: (i) the planarization of the molecule (i.e., inter-ring dihedrals decrease from 16° in **3T** to 10° in **3TO2**) and (ii) the strengthening of the C─C inter-ring bonds. S-Oxidized thiophene is clearly not a 6-π-electron system. Beyond disrupting aromaticity, accompanied by the upshift of the Raman bands, this central heterocycle becomes an electron deficient center, and some intramolecular charge transfer (ICT) from the outer electron rich thiophenes to the central electron withdrawing ring might be expected. Theoretical calculations actually predict a polarization of the atomic charge distribution from the outer thiophenes (+0.011 *e* in **3T** and +0.027 *e* in **3TO2**) to the central ring (+0.063 *e* in **3T** and +0.799 *e* in **3TO2**) upon sulfonation possibly due to the appearance of the ICT feature. If this ICT occurs, it requires a partial quinoidization of the structure that might necessitate planarization and strengthening of C─C inter-ring bonds. From the perspective of the molecular force field, it is known that planarization is able to promote increasing mixing of ring ν(C═C) and inter-ring ν(C─C) modes, these latter bonds being significantly strengthened upon sulfonation (1.450 vs 1.436 Å) as well as the C═C bonds according to calculations. Therefore, and as a result of the existence of ICT, the ν(C═C) modes are increasingly contributed to by inter-ring ν(C─C) modes which, due to their shortening, might push up by +14 cm^{-1} the wavenumber appearance of its associated Raman line.

The significant wavenumber downshift of the most intense line of the spectrum of **3Q** (1379 cm^{-1}) vs **3T** (1460 cm^{-1}) has been well explained in terms of quinoidization of aromatic oligothiophenes.[16] The strongest band at 1379 cm^{-1} (predicted at 1392 cm^{-1}) arises from a totally symmetric ν_s(C═C) vibration that spreads in the same way over the entire C═C/C—C conjugated path. In contrast, the medium intensity experimental band at 1512 cm^{-1} (calculated at 1513 cm^{-1}), which also arises from a ν_s(C═C) vibration, is mostly located at the terminal rings toward the CN groups.[29] Contrary to the case of **3T**, where the intense lines arise from ring stretching modes, in the quinoidal molecules the strongest Raman features emerge from oligoene-*like* C═C modes outlining the structural aromatic to quinoid evolution of the electronic structure. Another structural proof is the great lengthening of the C—S bond distances in **3T** vs **3Q**. Upon sulfonation of **3Q**, the Raman spectrum experiences a maximum upshift of 22 cm^{-1} in the case of the strongest line that is consistent with increased bond alternation (i.e., double bonds strengthen and single ones weaken). The thienyl BLA increases from −0.060 Å in **3Q** to −0.068 Å in **3QO2**, where the minus sign indicates the sequence of single and double bonds in the aromatic archetype is reversed in the quinoid. The changes on the DFT//B3LYP/cc-pVDZ bond lengths of **3QO2** are more moderate in the outer rings than in the center in accordance with the observation that the 1520−1490 cm^{-1} lines scarcely move at higher energies. Comparing both classes of compounds, changes upon sulfonation are larger in the aromatics where the S atom participates in the π-electron structure through ring aromatization. In the quinoids, however, S atoms play the role of electron donors toward the C═C/C—C path, and the degree of involvement in the backbone π-conjugation is much smaller. In this sense, oxidation in **3QO2** diminishes the intramolecular charge transfer (vide infra) from the central electron-rich backbone to the outer dicyano electron-withdrawing groups since the removal of the electron-donor S atom (i.e., the ν(C≡N) lines, whose wavenumber lowers for increasing electron density on the cyano group, going from 2210 cm^{-1} in **3Q** to 2220 cm^{-1} in **3QO2**).[30]

D. On the Raman Intensities upon Sulfonation. The very high oscillator strength of the $S_0 \rightarrow S_1$ excitation (HOMO → LUMO one-electron promotion, vide infra) likely gives the largest contribution to the induced dipolar moment transition and of change of the molecular polarizability (at least for excitations in the preresonance region of our Raman experiment at λ_{exc} = 1064 nm) upon interaction with an electromagnetic field. Although this is a drastic simplification of the Raman phenomenon, it provides a qualitative picture to account for the Raman intensity changes between **3T** and **3TO2**.[31] The orbital topologies of the HOMO orbitals (i.e., greatly involved in S_0, Figure 7 vide infra) are quite similar, while the LUMOs in **3T** and **3TO2** (greatly involved in S_1) display significant differences for the central ring. Topologies for the external moieties in both compounds are quite similar. Hence, it can be argued that the **3T** → **3TO2** inversion of the Raman profile regarding the ν(C═C) lines is consequent to perturbation of the LUMO orbital (i.e., π(aromatic) → σ(S—O) role change of the lone electron pair of the central sulfur atom). Contrary to the aromatics, for the two quinoidals the ν(C═C) intensity profile is preserved upon sulfonation in accordance with the slight alteration of the HOMO/LUMO wave functions.

(29) It must be noted that the intense band at 1348 cm^{-1} likely emerges as the result of the lending of intensity by part of the 1392 cm^{-1} line through coupling with the CH_2/CH_3 deformation vibrations of the butyl groups. The butyl → ethyl substitution in the model could explain the absence of this feature in the theoretical spectrum.

(30) (a) Takenaka, T. *Spectrochim. Acta, Part A* **1971**, *27*, 1735. (b) Girlando, A.; Pecile, C. *Spectrochim. Acta, Part A* **1973**, *29*, 1859.

(31) Long, D. A. *The Raman effect. An unified treatment of the theory of Raman Scattering by molecules*; John Wiley & Sons: Chichester, 2002.

Table 2. Redox Potentials for the Trimers

	3T[a]	3TO2[a]	3Q[b]	3QO2
E_{red}		−1.65	−0.15	−0.07
E_{ox1}	1.05[c]	1.25	1.27	1.77
E_{ox2}			1.96	

[a] From ref 17. [b] From ref 14. [c] Irreversible oxidations (E_{pa} values provided). Working electrode: glassy carbon. Reference electrode: Ag/AgCl. Counter electrode: Pt wire.

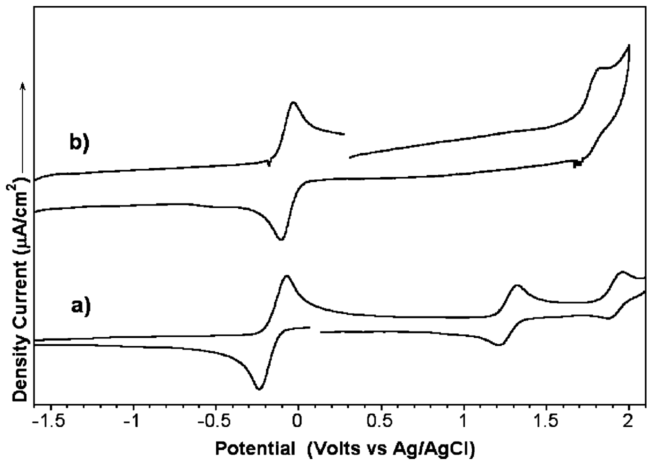

Figure 5. Cyclic voltammograms of (a) **3Q** and (b) **3QO2** in 0.1 M $TBAPF_6$ in CH_2Cl_2.

IV. Electrochemical Properties and Occupied and Unoccupied Molecular Orbitals

Cyclic voltammograms (CVs) of the oligomers were measured in 0.1 M $TBAPF_6/CH_2Cl_2$ solution, unless otherwise specified. Table 2 compares the redox potentials for the four oligomers.

As previously reported, **3T** displays an irreversible oxidation process at 1.05 V due to the reactivity of its cation radical. Upon sulfonation, this oxidation process shifts to higher energies, a trend common to oligothiophene sulfones and consistent with their affinity increments in the *S,S*-dioxides.[11] Similar trends are also observed for the redox properties of the quinoid system upon sulfonation (Figure 5). For example, the oxidation potential for **3QO2** (1.77 V) is much higher than that for **3Q** (1.27 V). In addition, sulfonation shifts the reduction processes of **3QO2** to less negative values with respect to **3Q**. Noteworthy is the magnitude of these changes. The relatively small change in the potentials of the reduction processes (0.08 V) is in sharp contrast to the large difference in the potentials of the oxidation processes (0.50 V). This demonstrates sulfonation in quinoid systems has a larger influence on the HOMO rather than the LUMO which will be discussed further in light of MO calculations (vide infra).

DFT//B3LYP/cc-pVDZ theoretical energies of the frontier orbitals (Figure 6) are used within Koopmann's approach to rationalize the evolution of experimental oxidation and reduction values.[32] Topologies for these orbitals are sketched in Figure 7. As for the aromatics, LUMO energies are much more stabilized

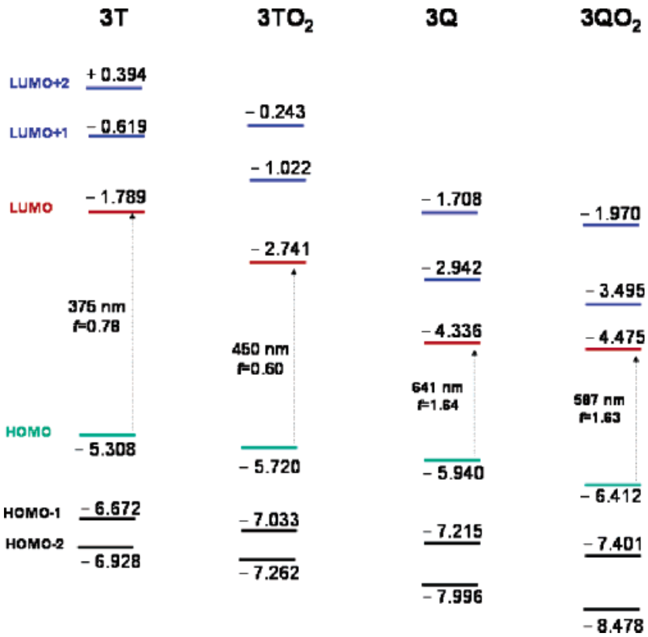

Figure 6. DFT//B3LYP/cc-pVDZ energy diagram for the orbitals around the gap. Energy transitions and oscillator strengths for the more important one-electron promotions are shown.

by sulfonation than are the HOMO energies, as observed in the cathodic processes. Reduction becomes possible in **3TO2** and is theoretically accounted for by the ~1 eV stabilization of its LUMO energy relative to **3T**. Moreover, the LUMO topology of **3TO2** reveals the important bonding interaction occurring in the central ring (i.e., absent in **3T**) likely responsible for its stabilization and cathodic activity.

At this point, it is possible to use electrochemical data and theory to support the spectroscopic finding in the Raman section for ICT in **3TO2**. Cyclic voltammetry indicates that the color-determining absorption band in **3TO2** at 2.89 eV (vide supra) can be identified as an intramolecular charge transfer transition because its transition energy is roughly equal (2.90 V) to the HOMO−LUMO gap (estimated from the difference between the first oxidation and first reduction waves). The bonding interaction predicted for the LUMO of **3TO2** is analogous to that noticed in the LUMO+1 orbital of **3QO2**.

Assuming that reduction consists of the incorporation of new electrons in the lowest unoccupied molecular orbital, then there is a much smaller influence in the reductions of **3QO2** than in that of **3TO2**. In this regard, a more moderate 0.1 V shift between **3Q** and **3QO2** is observed (~0.1 eV LUMO stabilization predicted by theory). Nonetheless, it must be highlighted that substitution of the aromatic backbone with electron-deficient dicyanomethylene or sulfone groups readily promotes reductions in a great range of cathodic potentials and is relevant for the engineering of these electroactive molecular materials. The contrary situation, however, is noticed for the orbital topologies of the HOMOs. No contribution from the central sulfur atom is predicted to the HOMO in **3T**. In **3Q**, the central sulfur supposes an additional node of the HOMO wave function that is removed upon formation of S−O bonds in **3QO2** resulting in its net stabilization and a concomitant increment of the electrochemical potential. This is a concise molecular interpretation of the tuning of the electrochemical properties by sulfonation and/or quinoidization of oligothiophenes.

V. Optical Spectra and Excited-Electronic States

A. UV−vis Absorption Spectra. The UV−vis spectra of **3T** and **3TO2** are characterized by an intense and featureless band centered at 357 and 428 nm, respectively (Figure 8). Table 3 summarizes the optical data discussed in the manuscript for the four studied molecules. Time-dependent DFT//B3LYP/cc-pVDZ calculations of the excited states have been obtained for the four compounds. Theory also predicts the appearance of an intense transition at 375 nm (oscillator strength, f, of 0.78) in **3T** and at 450 nm (f = 0.60) in **3TO2** with each component corresponding almost exclusively to a one-electron HOMO → LUMO excitation.

The significant red-shift of this band upon sulfonation of the aromatic backbone is mainly accounted for by stabilization of the LUMO orbital (i.e., bonding interaction within the central ring) such as the case described in the electrochemical section. Although the HOMO of **3TO2** is stabilized upon sulfonation, the greater LUMO stabilization dominates the HOMO−LUMO gap change from **3T** to **3TO2**. The π to σ conversion of electron density of the central sulfur atom might decrease the extent of the dipolar reorganization that occurs along with the HOMO → LUMO ($\pi\rightarrow\pi^*$) excitation. This fact is probably responsible for diminishing oscillator strength from 0.78 to 0.60 between **3T** and **3TO2**. On the other hand, the bonding interaction in the LUMO **3TO2** might stabilize the charge density in the central ring upon $S_0 \rightarrow S_1$ photoexcitation, an effect that is apparently absent in **3T**, and that can be viewed as distinctive proof of the existence of an ICT in the sulfonated compounds as already outlined in previous sections.

A significant red-shift of about 300 nm is noticed upon dicyanomethylene capping and subsequent quinoidization of the aromatic terthiophene; furthermore molar absorptivity for the low lying energy band changes by 1 order of magnitude from **3T** (i.e., 1.6×10^4 M^{-1} cm^{-1}) to **3Q** (i.e., 1.3×10^5 M^{-1} cm^{-1}).[14] This results from the increased acceptor character of **3Q** upon substitution with a strong acceptor group (i.e., LUMO energy stabilization) and the extension of π-conjugation to these external groups through their additional C=C−C≡N paths (i.e., HOMO energy destabilization). The overlapping of these two effects confers to this band a subtle character of intramolecular charge transfer (ICT) manifesting as a strong absorbance gain of this HOMO−LUMO band in the quinoidal systems compared to the aromatic homologues. In contrast to the comparison of **3T** to **3TO2**, however, sulfonation enlarges the optical gap by 85 nm. These results can be interpreted by a careful analysis of the origin of the electronic transitions.

The UV−vis absorption spectra of **3Q** and **3QO2** are characterized by one very intense and structured band at 670 nm ($\epsilon = 1.3 \times 10^5$ M^{-1} cm^{-1}) and 585 nm ($\epsilon = 1.1 \times 10^5$ M^{-1} cm^{-1}), respectively.[14] Theoretical calculations for **3QO2** predict the occurrence of the lowest lying energy band at 587 nm, by far the strongest band of the spectrum (f = 1.62) and corresponding to a one-electron HOMO → LUMO excitation. TD-DFT//B3LYP/cc-pVDZ also predicts, with reasonable accuracy, the position and intensity of this excitation in **3Q**, namely, 641 nm and f = 1.64, while they share the same HOMO → LUMO nature of their aromatic homologues. The depression of the

(32) Koopmans, T. *Physica* **1933**, *1*, 104.

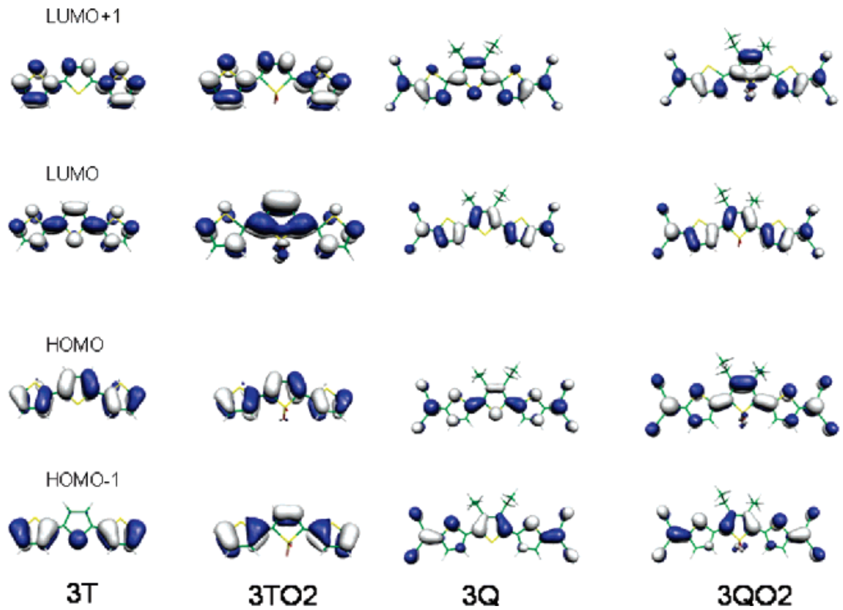

Figure 7. DFT//B3LYP/DZVP molecular orbital topologies for the most relevant terms of each compound.

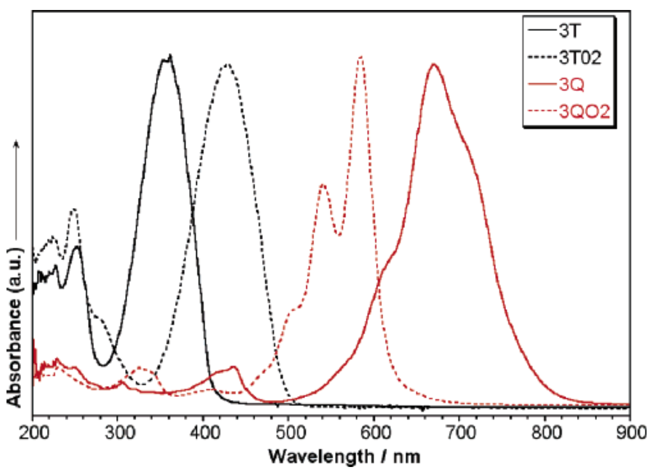

Figure 8. Normalized UV–vis electronic absorption spectra of **3T**, **3TO2**, **3Q**, and **3QO2** in CH_2Cl_2.

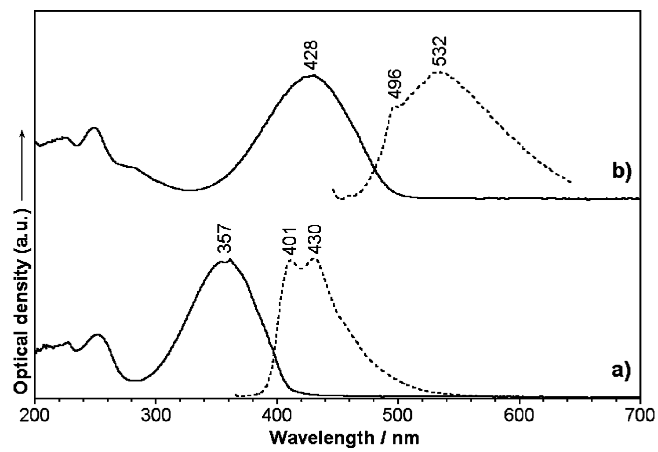

Figure 9. Absorption (solid line) and fluorescence spectra (dotted line) of (a) **3T** and (b) **3TO2** in CH_2Cl_2.

Table 3. Optical Data for the Studied Compounds in Dichloromethane

	3T	3TO2	3Q	3QO2
absorbance	357	428	670	585
emission	401/430	496/532		
FQY[a]	0.065	0.00035		

[a] FQY: Fluorescence quantum yield.

HOMO energy of **3QO2** (see Figure 6) is due to removing the lone electron pair of the central sulfur from the π system, enlarging the HOMO–LUMO gap. This fact, however, scarcely affects the oscillator strength in both quinoidal systems in line with the ICT character of this band that is governed by the CN acceptors.

The pronounced vibronic structure of the UV–vis absorption spectrum of the sulfonated quinoid is also observed in **3Q** but with much less resolution. Rigidifition and planarization of the ground electronic state in both quinoidals likely cause these effects. Furthermore the vibronic activity in the UV–vis absorption spectra of **3Q** and **3QO2** correlate with the vibronic structure of the fluorescence spectra (vide infra, Figure 9) of the aromatic homologues where the emissive S_1 electronic state has a pronounced quinoidal character such as the case of the absorptive S_0 state in **3Q** and **3QO2**. The close connection between the electronic and vibrational properties, or vibronic features, is nicely exemplified by correlating the differences in energies of the consecutive vibronic peaks in the UV–vis to the wavenumbers of the Raman lines.[33] Thus, it is noted that the difference in energy between any two consecutive peaks in the absorption spectrum of **3QO2** is 1429 cm^{-1} which, within the experimental error, coincides with the strongest Raman line at 1402 cm^{-1}. This comparison is less successful in the case of **3Q** where the vibronic progression is clear for two shoulders of the central peak, spaced by 1386 cm^{-1}, that correlates with the strongest Raman line of **3Q** at 1392 cm^{-1}. This substantiates that the photophysical properties of these systems are dominated by the interplay between quinoid (S_0) and aromatic (S_1) electronic structures and are strongly mediated or coupled through C=C/C–C stretching modes whose Raman activity is extraordinarily enhanced.

(33) Lanata, M.; Bertarelli, C.; Gallazzi, M. C.; Bianco, A.; Del Zoppo, M.; Zerbi, G. *Synth. Met.* **2003**, *138*, 357. D'Amore, F.; Lanata, M.; Gallazzi, M. C.; Zerbi, G. *Chem. Phys. Lett.* **2003**, *377*, 243.

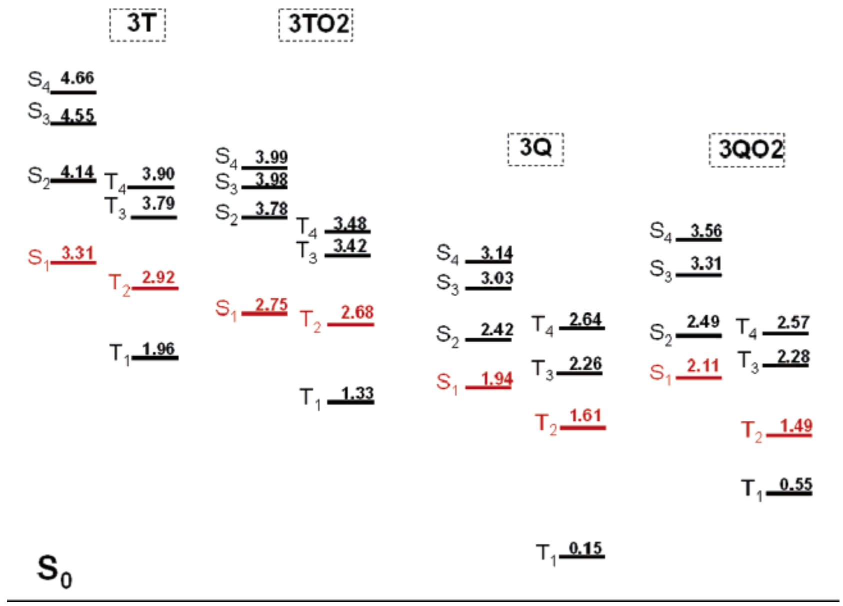

Figure 10. TD-DFT//B3LYP/cc-pVDZ energy diagram showing the relative dispositions of the singlet and triplet manifolds. In red, the relevant terms for intersystem crossing.

B. Emission Spectra. Figure 9 displays the absorption and fluorescence emission spectra of **3T** and **3TO2**. Three main features are noticed: (i) Both emission spectra are vibronicly structured (two resolved peaks in each spectrum). (ii) Similar Stokes shifts are measured for **3T** (4755 cm^{-1}) and for **3TO2** (4567 cm^{-1}). Provided that emissions proceed through the S_1 states of each molecule (i.e., section V.A. about the $S_0 \rightarrow S_1$ excitation or one-electron HOMO → LUMO promotion), this first singlet excited state is expected to adopt a quinoid planar rigid geometry in **3T** and in **3TO2** (i.e., the CC bonding features in the LUMO wave functions appear over the inter-ring bonds). The overall dominance of structural changes affecting the C=C/C−C path in both compounds is at the origin of their similar band features and Stokes shifts. (iii) Fluorescence quantum yields decrease upon sulfonation from $\Phi = 0.065$ in **3T** to $\Phi = 0.00035$ in **3TO2**.

Previous works have reported the increase of solid-state photoluminescence upon *S,S*-dioxide incorporation in the oligothiophene chain, a phenomenon not extensible to the solution phase.[11] It has been argued that the main route of fluorescence quenching in solution might be due to the nonradiative $S_1 \rightarrow S_0$ internal conversion (IC) seemingly promoted by the decreasing S_1-S_0 energy gap upon sulfonation of the aromatic thienyl backbone.[34] This IC mechanism seems unaffected by environment polarity, and therefore coupling between the dipolar moment induced in the molecule by oxidation and the solvent is excluded to affect the radiative decay. In this regard, an examination of the singlet/triplet manifold for intersystem crossing should also be inspected in order to account for this fluorescence change after sulfonation. Additionally, new explanations should be considered since the quinoidal S_1-S_0 energy gap is enlarged upon sulfonation and the hypothesis of increasing $S_1 \rightarrow S_0$ IC would be ruled out. Consequently, the following discussion seeks a unified interpretation of the emission properties of these molecules and the possible significance in the design of new electroluminescent organic compounds.

At the structural level, the role of sulfonation is the quenching of fluorescence emission. Figure 10 compares the relative disposition of the singlet and triplet manifolds for **3T**, **3Q**, **3TO2**, and **3QO2** as deduced by TD-DFT//B3LYP/cc-pVDZ calculations. In this regard, $S_1 \rightarrow T_n$ intersystem crossing, detrimental to fluorescence, is ruled by two main factors: (i) the large S−T energy gaps (i.e., low E_g^{S-T} favors S → T crossing); and (ii) the spin−orbit coupling which depends mainly on the presence of heavy atoms.

Upon vis photoexcitation, $S_1 \rightarrow T_2$ intersystem crossing can occur with the smallest *activation* energy $E_g^{S_1-T_2}$ of 0.39 eV in **3T** and $E_g^{S_1-T_2}$ of 0.07 eV in **3TO2** indicating that sulfonation effectively quenches fluorescence emission as observed in the experiments. This description is consistent with previous works: (i) Becker et al. have studied the photophysical properties of oligothiophenes and conclude that the singlet−triplet ISC is the main nonradiative process occurring in solution being especially important in the shortest chain members.[3a,b] (ii) Beljonne et al. have considered explicitly the spin−orbit factor in the ISC rate and conclude that the dominant contributions to ISC result from the presence of triplet states located close in energy to the lowest singlet excited state (this is our main argument).[5e] In this regard, (iii) the largest contribution to the ICS rate constant in oligothiophenes is controlled by the S−T energy gaps considering that the spin−orbit term would be large enough due to the heavy atom effect.

The two quinoidals show negligible emissive properties both in solution (i.e., $\Phi = 3.669 \times 10^{-6}$ for **3Q** to $\Phi = 1.260 \times 10^{-5}$ for **3QO2** both in dichloromethane) and in the solid state. In this regard, an additional argument to evaluate the emission properties of these compounds is that rotation of the rings along the conjugated segments in the excited states will considerably enhance the spin−orbit couplings and hence the probability for intersystem crossing.[5] In the case of the aromatic molecules this contribution must be ruled out because of the rigid structure of

(34) Anni, M.; Della Santa, F.; Raganato, M. F.; Fabiano, E.; Lattante, S.; Cingolani, R.; Gigli, G.; Barbarella, G.; Favaretto, L.; Görling, A. *J. Phys. Chem. B* **2005**, *109*, 6004. Raganato, M. F., Vitale, V.; Della Santa, F.; Anni, M.; Cingolani, R.; Gigli, G.; Favaretto, L.; Barbarella, G.; Weimer, M.; Görling, A. *J. Chem. Phys.* **2004**, *121*, 3784. Della Santa, F.; Gigli, G.; Raganato, M. F.; Anni, M.; Pisignano, D.; Cingolani, R.; Favaretto, L.; Sotgiu, G.; Barbarella, G.; Antolini, L. *Org. Electron.* **2004**, *5*, 129.

the quinoidal S_1 excited state. In contrast, this is the key situation in the case of the quinoid molecules. The inversion of the wave function patterns of the HOMO/LUMO orbitals in going from the aromatic to the quinoidal molecules gives rise to a LUMO orbital in **3Q**/**3QO2** where the π-electron features are antibonding for the inter-ring C−C bonds, conferring a great degree of rotational freedom to the skeletal backbone in the first lying excited state. This degree of S_1 conformational distortion might be enhanced by the steric crowding of butyl groups in the central ring of **3Q** and **3QO2**.

Regarding the energetic term of the ISC rate, the singlet and triplet manifolds in the quinoid molecules (Figure 10) show that the energy difference between the S_1 and the closest lying T_2 state goes from $E_g^{S_1-T_2} = 0.33$ eV in **3Q** to $E_g^{S_1-T_2} = 0.62$ eV in **3QO2**. These data further indicate that, relative to the aromatic homologues, the overall fluorescence is seemingly favored for the quinoid systems (i.e., larger $E_g^{S_1-T_2}$ terms). If the $S_1 \rightarrow S_0$ IC term is invoked here, as by Barbarella et al.,[34] fluorescence would be expected to increase along with the S_1-S_0 gap. Consequently sulfonation could enhance emission more in **3Q** than in **3T**.

Taking into account the observation of fluorescence quenching in these quinoidals, it must be assumed that the overall ISC rate constant is dominated by the term of spin−orbit coupling over the $E_g^{S_1-T_2}$ term. Therefore, the distortion of the conjugated backbone in the S_1 state is the main explanation for the effective ISC rate followed by the disappearance of fluorescence. This conclusion is further supported by two more experimental findings: (i) A more viscous solvent would hinder annular rotation in the S_1 state, and fluorescence emission should be favored. This is actually measured for the two quinoidals in decaline where quantum yields are $\Phi = 1.433 \times 10^{-4}$ for **3Q** and $\Phi = 5.565 \times 10^{-4}$ for **3QO2**. (ii) The observation of fluorescence (i.e., $\Phi = 1.571 \times 10^{-4}$) in an analogue quinoid terthiophene, **3QH3** (i.e., 5,5′′-bis(dicyanomethylene)-3,4′,4′′-trihexyl-5,5′′-dihydro-2,2′:5′,2′′-terthiophene). In this case steric hindrance in S_1 impedes rotation around the inter-ring bonds diminishing ISC crossing. (iii) Upon reduction of **3Q** and **3QO2** with triethylamine both samples intensively emit, in agreement with the discussion about the influence of the conformational effects in the overall fluorescence.

A starting hypothesis for improving light emission in efficient electron-accepting quinoidal systems would be rigidification of the thienyl backbone, for example, by adding saturated bridges between consecutive rings. In this S_1 planar compound sulfonation would further contribute to the overall fluorescence. Note that the capacity for ambipolar electron and hole conduction, critical to achieving charge compensation in electroluminescent materials, implies even weakly emissive molecules in order to attain very promising electroluminescent materials (i.e., this is the opposite concept to the attainment of great emitters which are poor charge transporters).

VI. Conclusions

We have examined the electronic and molecular structures of two pairs of aromatic and quinoid terthiophenes in both the ground and excited states. Vibrational Raman, UV−vis absorption, fluorescence, electrochemistry, and DFT/TD-DFT theoretical calculations characterized the π-system. Two main effects are addressed: (i) the consequence on the molecular and electronic structures of the aromatic to quinoid tuning of the oligothiophene backbone and (ii) the effect of sulfonation of the central sulfur atom in both quinoid and aromatic systems. This last case is quite interesting since sulfonation of oligothiophenes has resulted in significant photoluminescence in the solid state. This is remarkable because this effect is only noticed for solids, while solutions exhibit emission quenching.

Quinoidization of aromatic terthiophene results in the appearance of amphoteric redox behavior and a considerable reduction of the optical gap. Very interestingly the aromatic to quinoid structural change involves the *inversion* of the wave function profiles of the HOMO and LUMO frontier orbitals. Thus aromatic and quinoid samples behave complementarily regarding their optical and electronic properties: (i) **3T** is a good electron donor, and **3Q** is better electron acceptor. (ii) **3Q** absorbs in the vis(red)−NIR region, while in **3T** the absorption is displaced to the other side of the vis region of the spectrum. (iii) Sulfonation of **3T** results in red-shifting of the optical gap, whereas in **3Q** causes blue-shifting. (iv) Aromatic oligothiophenes strongly fluoresce (i.e., mitigation of the ISC rate due to S_1 conformational rigidification), while emission in quinoidal molecules is quenched efficiently (i.e., exaltation of ISC rate by S_1 conformational flexibility). It must be stressed, however, that far from an antagonistic description of these features, due to the similar chemical natures of these two classes of oligothiophene molecules, their properties would be combined, for example, to cover a broad range of optical absorption and emission, or to tune their electrochemical potentials extending from the cathodic to the anodic branches.

Sulfonation of terthiophene de-aromatizes the central thiophene which becomes an electron acceptor center promoting an intramolecular charge transfer from the outermost electron rich rings. This ICT likely accounts for the significant red-shifting (∼70 nm) of the lowest lying electronic absorption noticed for **3TO2** vs **3T**. In the case of the quinoid terthiophene, oxidation deactivates the electron donor ability of the central sulfur and gives competing ICTs (i.e., from the central **3Q** backbone toward the outermost dicyanomethylene groups and from the outer thiophene rings toward the central one in **3QO2**). Electron affinity, on the other hand, is improved in **3QO2** with respect to **3Q**.

Sulfonation of oligothiophenes has proven to be effective in promoting solid-state photoluminescence; therefore a careful understanding of the fluorescence properties of these compounds has been attempted. Two main factors control the emissive features: (i) the flexible/rigid properties of the ground/first-excited states of **3T** and **3Q**. In this regard, the more probable fluorescence deactivation channel in these systems has been proposed which is seemingly controlled by the energy gap between the S_1 and the T_2. Steric crowding plays also a subtle role in the excited state of the quinoidal molecules. Surprisingly sulfonation of **3T** promotes emission quenching of S_1 in solution, whereby the observed photoluminescence increasing in solid states likely has an intermolecular origin. Predicted light emission gain upon sulfonation of **3Q** offers luminescence enhancement in extremely efficient electron/hole conductors. This is of great interest for new electroluminescent organic materials. The rigidity of the conjugated backbone through the β, β' positions of thiophene in quinoid molecules can facilitate this goal.

Acknowledgment. J.C. is grateful to the Ministerio de Educación y Ciencia (MEC) of Spain for a Ramón y Cajal research position of Chemistry at the University of Málaga and for funding the stage at NRC through the fellowship PR2006-0253 of the Programa Nacional de Ayudas a la Movilidad de Profesores e Investigadores en el Extranjero. The present work was supported in part by the Dirección General de Enseñanza Superior (DGES, MEC, Spain) through the research project BQU2003-03194. We are also indebted to Junta de Andalucía (Spain) (FQM-0159) for funding our research group.

Supporting Information Available: Reference 21 and crystallographic and refinement data for **3QO2** are provided; crystallographic data in CIF format for **3QO2**. This material is available free of charge via the Internet at http://pubs.acs.org.

JA061372W